Materials Today Physics 46 (2024) 101504

Contents lists available at ScienceDirect

Materials Today Physics

journal homepage: www.journals.elsevier.com/materials-today-physics

Local probing of the nanoscale hydration landscape of kaolinite basal facets in the presence of ions

Clodomiro Cafolla [a,**], Tai Bui [b,c,d], Tran Thi Bao Le [e], Andrea Zen [f], Weparn J. Tay [d], Alberto Striolo [e,g], Angelos Michaelides [b,c,h], Hugh Christopher Greenwell [i,***], Kislon Voïtchovsky [a,*]

[a] Physics Department, Durham University, Durham, DH1 3LE, UK
[b] Thomas Young Centre and London Centre for Nanotechnology, London, WC1H 0AH, UK
[c] Department of Physics and Astronomy, University College London, London, WC1E 6BT, UK
[d] BP Exploration Operating Co. Ltd, Thames, TW16 7LN, UK
[e] Department of Chemical Engineering, University College London, WC1E 7JE, London, UK
[f] Dipartimento di Fisica Ettore Pancini, Università di Napoli Federico II, Monte S. Angelo, I-80126, Napoli, Italy
[g] School of Sustainable Chemical, Biological and Materials Engineering, University of Oklahoma, Norman, OK, 73019, USA
[h] Yusuf Hamied Department of Chemistry, University of Cambridge, Cambridge, CB2 1EW, UK
[i] Chemistry Department, Durham University, Durham, DH1 3LE, UK

A B S T R A C T

The interface between aqueous solutions and the facets of kaolinite plays an important role in a wide range of technological applications including tribology, paper production, oil recovery, waste water treatment and medical devices. This is made possible by kaolinite's layered structure, with its two basal surfaces -aluminol and siloxane-exhibiting different properties and reactivity. Using a combination of high-resolution atomic force microscopy (AFM) and atomistic molecular dynamics (MD) simulations, we probe *in situ* the hydration structure over both facets, in water and in the presence of added NaCl. The AFM images reflect the facets' first hydration layer, as confirmed from simulations. Complementary AFM spectroscopy measurements show an excellent agreement between the conservative component and MD's water density profiles, with discrete hydration layers on both facets and little sensitivity to added ions. The dissipative component of the measured tip-sample interactions is more sensitive to the presence of ions, with MD suggesting a link with the local water dynamics and transient instabilities between stable hydration layers. These effects are facet-dependant and more pronounced on the aluminol facet where the first water layer is better defined. Increasing the salt concentration allows hydrated ions to form more stable layers, with hints of organised ionic domains. The results provide unique insights into both the equilibrium molecular structure and dynamics of the kaolinite facets, potentially informing applications involving interfacial processes.

1. Introduction

Kaolinite is one of the most abundant natural clay minerals within soils at the Earth's surface and within rock units in the upper crust [1,2]. It plays important roles in technological developments ranging from pharmaceutical applications as excipient or active ingredient [3,4] and medical coagulative testing [5], to enhanced oil recovery [6,7], tribology [8], ceramics [9,10], wastewater and nuclear treatment [11,12]. The wide range of uses and applications of kaolinite is directly connected to the physical properties arising from its asymmetric layered structure, as well as its abundance. Kaolinite (chemical formula $Al_2Si_2O_5(OH)_4$) is a layered 1:1 clay mineral, with each layer made of two different sheets [13]: a tetrahedral siloxane sheet and an octahedral aluminol sheet, linked through shared coordination oxygens atoms [13,14] (Fig. 1). This asymmetry results in the layers being strongly dipolar, with large dipole-dipole stacking interactions [13,15]. Hydrogen-bonds can further contribute to attractive interactions between the siloxane surface of a layer to the aluminol surface of a neighbouring layer. This promotes inter-layer interactions and structuring of the mineral into platelets. Platelets constitute the crystallographic unit of kaolinite and can form larger aggregates [13], even when kaolinite particles are dispersed in water and aqueous systems [16].

The combined effect of dipolar and electrostatic interactions ensures a strong cohesion among layers and makes the interlayer region difficult

* Corresponding author.
** Corresponding author.
*** Corresponding author.
E-mail addresses: clodomiro.cafolla@durham.ac.uk (C. Cafolla), kislon.voitchovsky@durham.ac.uk (K. Voïtchovsky).

https://doi.org/10.1016/j.mtphys.2024.101504
Received 6 March 2024; Received in revised form 30 May 2024; Accepted 8 July 2024
Available online 9 July 2024
2542-5293/© 2024 The Authors. Published by Elsevier Ltd. This is an open access article under the CC BY license (http://creativecommons.org/licenses/by/4.0/).

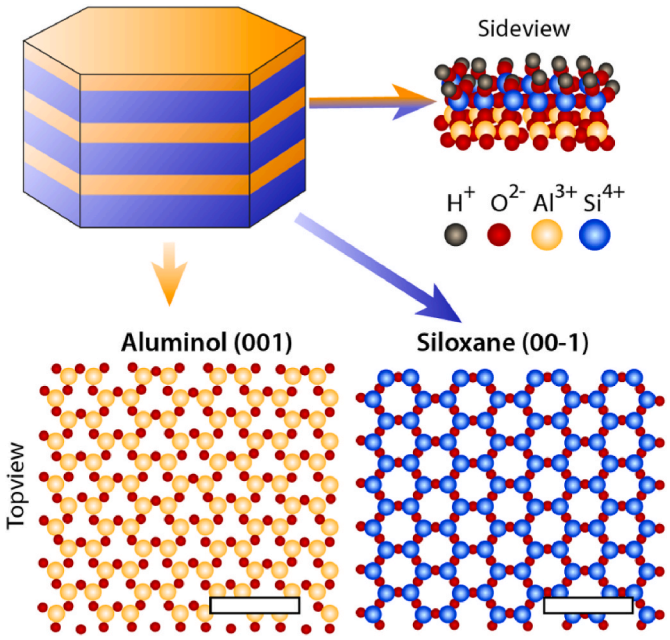

Fig. 1. Schematic representation of a kaolinite nanoplatelet as naturally occurring. Kaolinite is made of layers of aluminol octahedra and siloxane tetrahedra linked through shared coordination oxygens atoms [13]. The atomic arrangement of each layer is presented as seen from the top and from the side. The hydrogen atoms are not shown in the top view schematic. The sideview schematics highlights key differences in the spatial arrangement of the atoms of the two facets. In particular, the oxygen atoms of the siloxane surface do not all sit in the same plane. The scale bar represents 1 nm.

to access by molecules and ions from the surrounding environment. If accessed, the interlayer spacing provides a functional, asymmetric, and highly stable two-dimensional surface suitable for chemical reactions and physical processes. Examples span from wastewater treatment to oil droplets adsorbing at the interface with two anisotropic solid surfaces [13,14]. Accurately characterising the properties of these facets is therefore crucial, both at a fundamental level and to enable the rational design of kaolinite-based technologies. Traditionally, experiments on kaolinite have focused on a better understanding of the macroscopic chemical characteristics, mechanical properties and, above all, adsorption process and charging behaviour [17–23]. Potentiometric titrations and zeta potential measurements quantified the protonation and charging state of gibbsite particles, considered as analogues to the kaolinite aluminol facet. These investigations revealed the effects of different reaction times on proton uptake and zeta potential [19] and quantified metal adsorption [20]. Electrokinetic studies have investigated the zeta potential of kaolinite suspensions, showing a dependence on both salt concentration [22,23] and pH [22], although the impact of salt remains a matter of debate [21–23].

These experimenal approaches are, however, limited by the macroscale, average picture they provide, glossing over local effects due to surface chemical or physical singularities. Such effects are essential to understand short range phenomena such as hydration [24–28], molecular adsorption [24,29–31] and charging [32–34]. X-ray and solid-state nuclear magnetic resonance measurements [35,36] have helped resolve some of these phenomena, revealing the molecular coordination details around heavy metals and oxides adsorbed on kaolinite facets [37,38]. Results have evidenced ion-pairing and hydration energy as the two main factors that control the adsorption of mono-, di- and tri-valent ions onto kaolinite [39,40]. Interestingly, X-ray photoelectron spectroscopy and zeta-potential measurements showed both the siloxane and the aluminol facets to be negatively charged when immersed in pure water due to the deprotonation of SiOH/AlOH to SiO^-/AlO^- (pH < 7) [39,40].

Despite these interesting advancements, the complexity of the interfacial environment and the variety of phenomena occurring at the interface with kaolinite in the presence of water and different ions justify the need of molecular modelling to achieve a thorough understanding of the systems considered. Local nanoscale insights can in principle be obtained theoretically through computer simulations or experimentally with techniques using local probes.

Molecular dynamics (MD) simulations at the kaolinite-water interface have shown a sharp decrease of in-plane water diffusion close to the surface [41–43], with orientation-dependent water dynamics at the interface [41]. Adsorbed surface ions appear to have a significant impact on the hydration structure [44], with the ions' hydration energy determining the preferential adsorption state (inner-sphere or outer-sphere) on kaolinite's facets [45]. Classical MD simulations are however limited by the accuracy of the force fields available [46], and cannot explicitly account for pH effects [41–43]. *Ab initio* simulations can be instead used to determine the most energetically favourable surface terminations and partial charges distributions on neutral (protonated) and negatively charged (deprotonated) kaolinite surfaces which can then serve as a starting point for MD simulations [47]. This combined approach confirmed previous experimental results, showing that the deprotonation of the aluminol and silanol groups are energetically favourable at alkaline pH (above the point of zero charge). This makes kaolinite negatively charged in neat neutral pH with surface groups including two $AlOH^{-1/2}$ and one SiOH per unit cell.

Experimentally, atomic force microscopy (AFM) has enabled local probing of interfaces, often in complementarity to MD simulations [48–50]. AFM measurements on kaolinite particles revealed the local topography [51,52], the average distribution of surface charges [33,34,51,53], and quantified *in situ* the isoelectric point for both facets with the siloxane tetrahedral face being at pH < 4, and for the aluminol octahedral facet lying between pH 6 and 8 [54–56]. AFM studies showed that the basal planes of kaolinite have a charge that varies with pH and salt concentration, in contradiction with macroscale studies which suggest both kaolinite facets to carry a permanent negative charge due to isomorphous substitution [54]. This contradiction can be explained by local surface singularities [33] and chemical defects [6] that influence the resulting charge distribution. High-resolution AFM measurements evidenced the impact of singularities on the local charge distribution [33], showing that simple surface complexation models assuming a unique and homogenous surface chemistry tend to fall short for describing important aspects of real kaolinite surfaces [34].

Both macroscopic and nanoscale studies point to a strong dependence of kaolinite's surface properties on its local hydration structure. No experimental results, however, have systematically and comparatively investigated the hydration landscape of both basal facets to date. Here, we carry out such an investigation, combining AFM and classical MD simulations with atomic-level resolution. This combined approach allow us to overcome the limitations of each technique via the advantages of the other. Specifically, AFM images highlight the differences in the first hydration layer of each facet and serve as a basis for force spectroscopy measurements of the full hydration profile at a given location [57]. Water densities extracted from MD help interpret the AFM results, both in the absence and in the presence of added Na^+ ions.

2. Materials and methods

2.1. Sample preparation

The sample preparation is based on the positively charged aluminol (negatively charged siloxane) facet of the kaolinite crystals being attracted to the negatively charged surface of muscovite mica (positively charged surface of sapphire) [6,34,54–56]. This allows preferentially exposing one or the other kaolinite facet to the AFM tip and exploring that specific basal face's interfacial properties when immersed in ionic aqueous solutions. High-quality V1 muscovite mica discs (SPI Supplies,

West Chester, PA, USA) and C Plane (0001) sapphire crystals (University Wafers Inc., Boston, USA) were glued to steel plates [29,58]. A suspension of the kaolinite powder (KGa-1b from the Clay Minerals Society Source Clay Repository) was prepared using ultrapure water (Water AnalaR NORMAPUR, VWR International Ltd, Leicestershire, UK). The final concentration of the suspension was 1.5 mg/ml. The pH of the kaolinite suspensions was adjusted to favour the charging of the desired facet and its consequent binding to the substrate of choice (mica or sapphire). When adsorbing the suspension to the muscovite mica, the pH was 6.8, whereas the pH for the adsorption to the sapphire substrate was 5.5.

The substrates were prepared as follows. The mica substrate was freshly cleaved and copiously rinsed with ultrapure water. The sapphire substrate was cleaned by rinsing with isopropanol (Sigma-Aldrich, St Louis, MO, USA), ethanol (Sigma-Aldrich, St Louis, MO, USA) and ultrapure water, and by exposure to low-pressure air plasma, at a pressure of 1 mbar and power of 300 W (VacuLAB Plasma Treater, Tantec) for 30 s [59–61].

50 mL of the kaolinite powder suspension was then drop casted onto the substrates. Both the mica and the sapphire substrates were incubated overnight at 40 °C, and then copiously rinsed with ultrapure water to remove loosely bound clay particles from the substrate [6,56].

The procedure for the selective exposion of the two facets follows similar protocols in the literature [6,56] and is furthermore confirmed observing the tip-surface interaction force changing as a function of salt concentration (see also Supplementary Information section 1 and Fig. S1).

2.2. Atomic force microscopy

AFM experiments were conducted at 25 ± 0.1 °C using a commercial Cypher ES equipped with temperature control (Asylum Research, Oxford Instruments, Santa Barbara, CA, USA). The AFM probes were Arrow UHF silicon nitride cantilevers (Nanoworld, Switzerland). The cantilevers were thoroughly washed with pure water (20 times with 100 μl) and then with the solution of interest (40 times with 100 μl). Experiments were performed at near neutral pH 5.8. This ensured that only the metal ions of interest were present on the cantilever. Thorough cleaning procedures were implemented to avoid any possible sources of contamination [28,58]. During the measurements, the cantilever and the sample were fully immersed in the aqueous ionic solution of interest. The thermal spectrum of the cantilever was used to perform the flexural calibration of the cantilevers [62]. The probes were found to have a flexural spring constant in the range 1.0–4.0 N/m and a resonance frequency of ~400–900 kHz in water. These values agree with the nominal range and the literature [29,63,64]. The cantilever oscillation was photo-thermally driven to ensure greater stability, making sure that the frequency response remained unaffected by any spurious contributions due to the noise produced by mechanical coupling with other experimental components of the system [65].

2.3. Imaging

An equilibrium picture of the kaolinite/aqueous solution interface was obtained operating the AFM in amplitude-modulation (AM) [24,58,66–69]. The oscillation amplitude was kept constant during imaging by a feedback loop constantly re-adjusting the average tip-sample distance. The topography is then reconstructed from the feedback corrections. The phase lag between the driving oscillation and the cantilever oscillation varied freely and carried information about the interactions between the tip and the interface [24,58,66–69]. All the data analysis was carried out using bespoke routines programmed in Python and Igor Pro (Lake Oswego, USA).

2.4. Force spectroscopy

Measurements were conducted dynamically (vibrating tip) and driven at oscillation amplitudes of ~0.2 nm, less than the thickness of a single hydration layer [29,70]. Only the selected interfacial region located immediately between the tip apex and the surface of the selected kaolinite region was interrogated during a spectroscopy measurement. High-resolution imaging was always conducted before and after force spectroscopy to rule out any surface damages or contamination and ensure that all the measurements were conducted at the region of interest [24]. For each facet investigated, 5 different locations were probed with at least 20 spectroscopic deflection, amplitude and phase vs distance curves per location. All the curves were acquired with an approach speed of 50 nm/s, aiming to explore distances smaller than the thickness of a water molecule within the relaxation time of the molecules themselves (1.1 ms and 5 ms, for the inner and diffuse layers of water, respectively) [71–73]. Out of all the acquired curves, the analysis focused on those showing an oscillatory profile (~30 % of the total), following the approach used in Ref. [51] where variability in the number of curves exhibiting an oscillatory profile was also reported. This can be explained by the stochastic nature of the measurement process, and the presence of chemical singularities and topographical defects on the kaolinite surface, in contrast to measurements conducted on defect-free mica and calcite surfaces [74,75]. To minimise the variability and mitigate its impact on the results we conducted the measurements on smooth terraces, sampling multiple locations in each case (see Supplementary Information section 2 and Figs. S2–3 for representative images of the locations probed).

For each facet, the same AFM tip was used to ensure quantitative comparability between the different salt concentration, with minimal impact from possible variations of the cantilever geometry on the force spectroscopy measurements. All the measurements on a given facet were carried out at the same location of the same clay particle. The experiments were performed increasing the salt concentration, starting from water and subsequently exchanging to the desired solution by replacement of the liquid through an inlet and an outlet 1 ml syringe connected to an otherwise fully sealed liquid perfusion cell. The exchange volume corresponds to at least 20 times the experimental solution volume (i.e. 20 replacement volumes). This exchange procedure provided complete removal of the previous solution while ensuring that all the measurements for a given facet were performed at the same location.

The conservative and dissipative components of the tip-sample interactions were calculated from the experimental data using established procedures [76] (see also Supplementary Information section 3 and Fig. S4). Determination of the point of contact between the tip and the sample (zero) was calculated for each curve as the tip-sample distance coinciding with the highest density of data points. With the data acquisition operating at a fixed rate, the highest density of data points within a 0.1 Å window represents the average tip position where moving closer to the sample is no longer possible due to a hard contact (atomic Pauli repulsion). Practically, a trigger was set on the average (DC) deflection of the cantilever, selecting a relatively low trigger value to prevent tip damage (<1 nN). The instantaneous contact between the tip and the surface remains intermittent due to the tip oscillation which creates a small offset and some uncertainty over the exact position of the zero so determined. The oscillation is however largely damped down to <0.1 nm (see for example the representative data in Fig. S4), resulting in a position error and offset smaller than 0.1 nm. Determination of the maximum density of data point was obtained from bespoke routines programmed in Igor Pro for every curve.

2.5. Molecular dynamics simulations

The experimental AFM techniques were complemented by classical MD simulations. These were preferred over *ab initio* MD simulations given the greater time and length scales they allow exploring. All the MD

simulations were conducted with the Large-scale Atomic/Molecular Massively Parallel Simulator (LAMMPS) software package [77]. In each periodic simulation cell, a slab of three layers of kaolinite (the crystallographic structure from Ref. [78]) was placed in the centre of the simulation box with 5000 water molecules on each side of the slab. Supplementary Fig. S5 depicts an image of the entire simulation cell, including the water molecules. The simulation box for the water-kaolinite slab was of 41.2 Å × 35.8 Å × 130 Å in volume. To minimise any size effects, a vacuum layer of 41.2 Å × 35.8 Å × 120 Å was added to the box along its z-direction. The simulations implemented the ClayFF potential [79–81] and the rigid SPC/E model [82] for kaolinite and water, respectively. The SHAKE algorithm was used to constrain the rigid water molecule and the OH distance in the kaolinite hydroxyl groups. Additional constraints on the kaolinite slab ensured the stability of the kaolinite slab restraining the heavy atoms (Al and Si) at their initial positions by means of a harmonic potential characterised by a spring constant of 10 kcal/(mol Å^2) [83]. To simulate a saline solution, NaCl ions were introduced into the system achieving a 1.2 M concentration. Na^+ and Cl^- ions were modelled as single-charged Lennard-Jones spheres following the model of Smith and Dang, albeit with no polarizability [84]. Interactions between different species were described using the standard Lorentz-Berthelot mixing rules based on the interaction parameters for the individual atoms. Real-space interactions with energy corrections were truncated at 10 Å, and a particle-particle-particle-mesh solver was employed to account for long-range electrostatics [85].

All the simulations were performed with a 1 fs time step. The system was equilibrated for 3 ns in the NVT ensemble at 25 °C using separate Nosé-Hoover chain thermostats for water and the kaolinite slab [86]. The system equilibration was confirmed by the convergence of the system potential energy and water oxygen density profiles (see Supplementary Information section 4 and Figs. S5–6). After equilibration, the simulations were run over a further 3 ns collecting the data. Here, the data included 1D and 2D density profiles and diffusion coefficients of the water molecules as a function of their distance from the kaolinite facets. The diffusion coefficients were calculated considering water molecules within slabs (20.0 Å × 20.0 Å x 3.0 Å), consecutively taken along the direction perpendicular to the kaolinite facets. The diffusion coefficients were extracted from molecules' mean square displacement curves using Einstein's relation [83].

3. Results and discussions

3.1. Mapping the facet's first hydration layer at equilibrium

Following established protocols (see Methods), kaolinite particles were stably deposited on a substrate to expose either of the two basal facets. Low resolution AM-AFM imaging was used to identify kaolinite particles (see Supplementary Figs. S2–3), with confirmation of the facet identity achieved through localized spectroscopy measurements: the evolution of the tip-sample interactions with increasing salt concentration follows classical DLVO predictions [54], enabling unambiguous facet identification (see details in Supplementary Fig. S1). High-resolution AM-AFM imaging then allows visualisation of the nanoscale details of the water-facet interfaces (Fig. 2). For comparison, the simulated water densities in the first hydration layer of both facets are shown side by side and to scale with the AFM images. In all images, a schematic of the anticipated atomistic arrangement is superimposed to scale.

The AFM images represent topographical maps of the hydrated surface of kaolinite immersed in water, with the higher regions appearing lighter, and using the same colour contrast as for MD to help visually

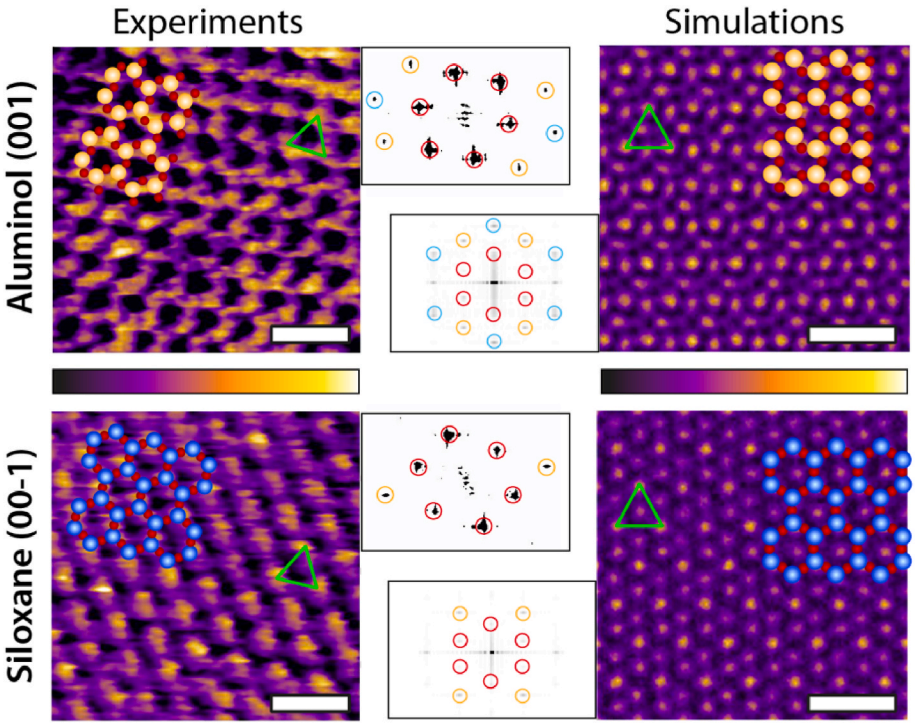

Fig. 2. Representative experimental (AFM) and computational (MD) images of both kaolinite facets. For each image, the corresponding atomic arrangement of the facet is superimposed to scale. The green triangle highlights the brightest periodic features appearing in both AFM and MD, showing a good agreement. The MD images represent the density distribution of the first hydration layer over each facet. The insets show the Fast Fourier Transform (FFT) of each image and highlight the first (red), second (orange) and third (cyan) order intensity peaks. The MD results represent a 2D projection for the water oxygen density in the first hydration layer averaged over 3 ns. The scale bar represents 1 nm. The AFM colour scale bar represents a height variation of ~0.3 nm; the MD colour scale is based on a density range at a fixed height (first hydration layer). (For interpretation of the references to colour in this figure legend, the reader is referred to the Web version of this article.)

compare the results. Experimentally, kaolinite was first equilibrated in ultrapure water, resulting in imaging a solution with a pH close to 6.8. When operated as in the present study, the AFM primarily maps the most stable hydration layer of the surface imaged [28,87,88], here the first hydration layer (see also the water density profiles in Fig. 3). This enables a direct comparison with MD simulations maps of the first hydration layer. The MD maps represent the distribution of the water oxygen atoms in the first hydration layer on each facet, with higher density regions appearing lighter (yellow-white colour).

The computational and the experimental approach show a relatively good agreement, particularly considering that the aluminol facet explored by the AFM is not perfectly planar (see Fig. 1 sideview schematics). On the aluminol facet, the octahedral atomic arrangement creates a hydration structure close to hexagonal symmetry, similar to a honeycomb pattern. However, the structure is slightly distorted, reflecting the in-plane position of the surface atoms (Fig. 1). In AFM, this is evidenced by the fact that the honeycomb cavities appear more triangular than hexagonal, a complexity reflected in the presence of higher order peaks in the image FFT (Fig. 2, inset). MD results offer hints to periodic cavities, but this is less clear due to the oxygen-bound hydrogen atoms being considered in the results displayed here. At the experimental pH [47], the water molecules on the aluminol facet can in principle probe more configurational states than on the siloxane facet due to an additional hydrogen group at the edges of the highlighted triangles: water molecules can bind directly the aluminol oxygen and hydrogen groups or interact with water molecules bound to the aluminol terminal groups. The combination of these possibilities yields a relatively denser first hydration layer by comparison with the one formed on the siloxane facet and gives rise to the apparent honeycomb lattice observed in the AFM images. On both facets, particularly bright protrusions are visible (highlighted by green triangles). The MD results indicate that they are due to a highly localized hydration shell above specific oxygen atoms (Fig. 2). The fact that these features are present in both AFM and MD suggests a good agreement between the techniques and confirms that AFM predominantly images the first hydration layer.

Over the silica facet, the atomic arrangement is easier to visualise as a simple honeycomb structure. This is strictly speaking not correct since not all the top-most atoms are in the same plane, leading to brighter features in both AFM and MD (green triangles). Aside from these subtleties, both techniques show a hexagonal lattice of hydration sites, resulting in fewer higher order FFT peaks. This is due to epitaxial effects [24,28] allowing water molecules to form hydrogen bonds with the oxygens of the siloxane pseudo-hexagonal lattice, an additional water molecule sitting at the centre of the hexagon with its dipole moment oriented perpendicularly to the surface. This is further confirmed by the lattice parameter measured in both the AFM and MD simulations maps and which closely matches the surface lattice parameter of 5.15 Å [89,90]. Generally, the AFM images over the siloxane facet appear slightly noisier than over the aluminol facet, consistent with the possibility that the siloxane-water interface exhibits a slightly less compact and less stable first hydration layer.

3.2. Probing the density and dynamics of hydration water

To gain quantitative insights into the behaviour of interfacial water, beyond the first hydration layer, it is helpful to consider the variation of quantities such as water density and diffusivity as a function of the distance from the topmost atoms of the kaolinite facets.

Experimentally, quantitative information can be derived from spectroscopy experiments. To ensure a high sensitivity to the hydration profiles, the AFM tip is oscillated with an amplitude comparable to or smaller than the size of a single water molecule [57]. As the vibrating AFM tip approaches the hydrated mineral surface, the tip oscillation is progressively damped, leading to changes in oscillation amplitude and phase (see Supplementary Information section 3 and Fig. S4 for further details). Eventually, the tip presses directly onto the mineral surface, leading to an average static (DC) deflection of the AFM cantilever. The conservative and dissipative components of the interactions experienced

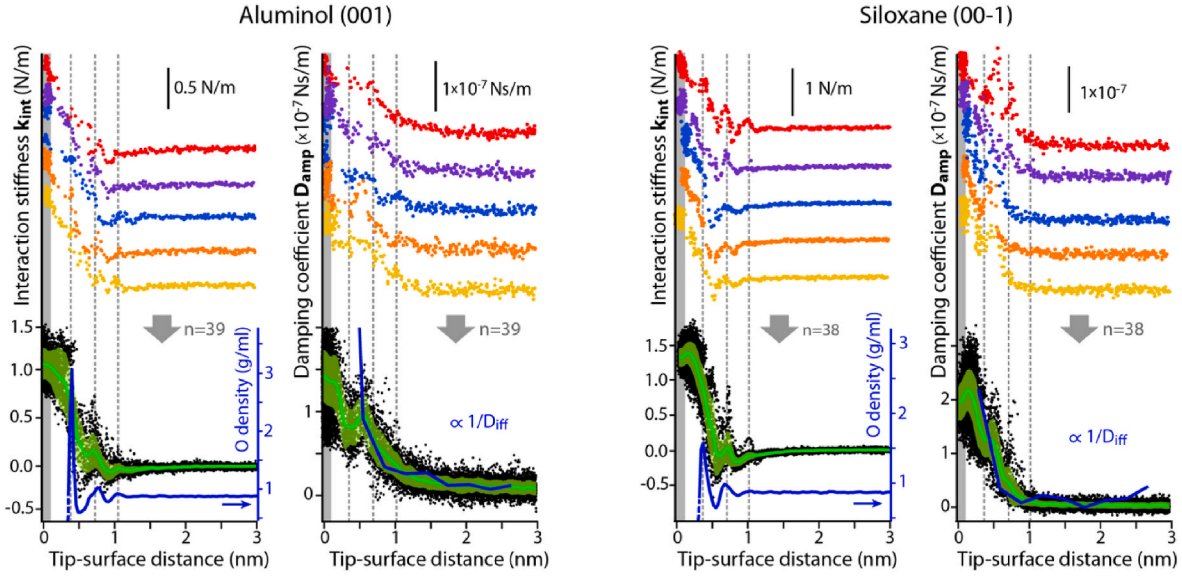

Fig. 3. Organisation and dissipation dynamics of the hydration water at the kaolinite interface. Representative AFM conservative (interaction stiffness) and dissipative (damping coefficient) spectroscopic curves are shown for the aluminol and siloxane facets immersed in pure water (top panels). The curves are vertically offset to help visual inspection. The condensed and fine-aligned experimental data (bottom panels) is averaged (green curves with semi-transparent thickness representing two standard deviations) and compared against MD results. The conservative component is compared with the MD density profiles for water's oxygen, and the dissipative with the MD-calculated inverse water molecular diffusivity. The dotted grey lines represent the position of the water layers from the local maxima in simulated water oxygen density profiles. For each facet, about 40 experimental curves are averaged, with the green shading around the average representing two standard deviations. The MD molecular diffusivity data has been inverted, offset to ensure zero at longer distances, and linearly rescaled to match the magnitude of the experimental dissipation data at 0.5 nm (see also Supplementary Information section 6). The shaded grey area around the origin of the plots represents the maximum horizontal offset used in the fine alignment of the experimental data. (For interpretation of the references to colour in this figure legend, the reader is referred to the Web version of this article.)

by the vibrating tip can be calculated from the changes in amplitude and phase as a function of the AFM tip-sample distance. Under the assumption of a locally harmonic interaction potential, the conservative component represents the interaction stiffness, proportional the conservative tip-sample force gradient. The dissipative component correlates with changes in the damping coefficient as experienced by the vibrating tip. The method, summarised and illustrated in Supplementary Information (section 3), follows an established approach described elsewhere [76]. Practically, multiple curves are acquired in at least five different locations of each solid-water interface with the conservative and dissipative components individually extracted from each set of curves. Given the inherently stochastic nature of molecular processes, a statistical approach is then used to identify the reproducible features, with the curves finely aligned (±1 Å) with respect to a common reference. The reference is obtained as the average tip-sample distance corrected with the static deflection of the cantilever. Most studies tend to focus on the conservative component of the tip-sample interaction where oscillations close to the mineral surface are interpreted in terms of densification and layering of the water molecules [57,73–75,91,92]. Consequently, the conservative part of the tip-sample interaction can be directly compared to the density profiles of the interfacial water as calculated by MD. Following this approach, we achieve a remarkable agreement between experimental and computational data (Fig. 3). Interestingly, on both facets, the water layers are found at similar distances from the kaolinite topmost atoms (~0.42 nm, 0.78 nm and 1.05 nm for the aluminol facet; 0.4 nm, 0.7 nm and 1.0 nm for the siloxane facet). It is worth highlighting that no significant post-alignment of the AFM and MD data needs to be performed with both the experimental and computational results naturally having their 'zero' that coincide within 1 Å in terms of tip-sample distance (adjustment over shaded grey region in Fig. 3). For the AFM measurements, the zero corresponds to the point where the oscillating tip reaches a hard contact with the surface during each oscillation cycle. Moving the base of the cantilever closer to the sample only results in a positive average (static) deflection of the cantilever but no further decrease of the average tip sample distance, within the tip oscillation amplitude. Given the significant damping of the free amplitude (~0.2 nm) at this point, the zero obtained by AFM lies within a fraction of the amplitude of the true zero (as determined by MD). In practice, the zero as determined by AFM spectroscopy can be objectively identified as the tip-sample distance with the highest density of data points (see Methods section). For the MD simulations the zero is given by the position of the topmost metal atoms of the aluminol/siloxane facets and is known by simulations design. This experimental strategy bypasses the usual arbitrary rescaling common to the most AFM spectroscopy measurements and offer an objective zero.

The two facets present key differences in the relative densification of the hydration shells. The MD results reveal a denser first hydration layer on the aluminol facet, leading to a sharper transition in the AFM conservative interactions with the tip apparently struggling to distinguish the strongly bound first hydration layer from the solid surface underneath (Fig. 3). This transition is less marked over the siloxane facet. From MD, the density peak associated with water oxygens has a maximum of ~3 g/ml and a width of ~0.2 nm compared to ~1.5 g/ml and ~0.3 nm for the siloxane interface. This leads to an average density of water of 1.26 g/ml and 0.82 g/ml on the aluminol and siloxane facets, respectively. The second hydration peaks are comparable on both facets, with the facets presenting density peaks of ~0.25 g/ml (aluminol) and ~0.30 g/ml (siloxane) and extending respectively up to ~ 0.4 nm and 0.3 nm further from the first layer (Fig. 3). This is consistent with existing literature [83,93] and with the similar but relatively small local maxima in the conservative curves. The fact that the density of the second hydration layer is an order of magnitude smaller than that of the first also supports the interpretation of the high-resolution AFM imaging of the interface (Fig. 2); attempts to image the second layer leads to significantly less stable images (Fig. S7).

Interpretation of the dissipative component of tip-sample interactions is usually less straightforward. Ongoing debates and sometimes contradictory results suggest possible dependence on the system being investigated [73,91,94]. Here, a maximum in dissipation often coincides with a position between the first two water layers, suggesting an increased dissipation as the measuring tip passes between cohesive layers. The absolute value obtained for the dissipation is similar on both facets, but with a maximum in dissipation more marked over the aluminol facet at a tip-sample distance ~0.5 nm. In fluid systems, dissipation can often be related to inter-molecular 'friction' or effective viscosity. To test this interpretation, we compared the dissipation data with the inverse of the water diffusivity obtained by MD. For a given fluid, molecular mobility, captured by Einstein diffusion coefficient, is inversely proportional to the viscosity (Stokes-Einstein [95]) and to dissipation (assuming a linear regime, see section 6 of the Supplementary Information for details, and Fig. S8 for the full MD data). Here, since we are primarily concerned with distance dependence from the facets, the water diffusivity obtained from MD is inverted and subsequently offset to ensure it converges to zero at longer distances (Supplementary Information section 6). The magnitude of the resulting curve is then linearly adjusted to match the dissipation at 0.5 nm (maximum of inter-layer dissipation). The adjustment at 0.5 nm is also motivated by the fact that no reliable diffusivity data is available from MD below 0.3 nm (see Fig. S8). While qualitative, the interpretation is physically justifiable, and correctly captures the longer-range effect of the dissipation compared to the conservative local water densification, with an increased effective viscosity reaching ~1 nm beyond the second water layer. Quantitative comparison of the magnitude of the dissipation between both facets should be carried out with some caution since different tips were used. The tips are composed of the same material, have the same design, are both able to achieve high-resolution (Fig. 2) and are from the same production batch, but atomistic differences exist. While such differences are unlikely to affect the shape of the stiffness and dissipation curves [96], they can influence the interaction dominating the measurements [97,98]. The emphasis is therefore placed on the shape of the curve, in particular the comparison between conservative and dissipative interactions for each facet where, *ceteris paribus*, the results show significant differences. A molecular-level interpretation of this increased 'effective viscosity' could be related to a larger number of dissipation channels available to water molecules located between -and able to probe- several stable arrangements [99]. Consistently, on the aluminol facet which first hydration layer appears particularly stable and well-defined from MD predictions, dissipation steps are more marked between the first and second water layer. If no stable hydration layers are present (here region where $z > 1$ nm), dissipation could be interpreted as inversely proportional to the local molecular mobility. Further studies are however needed to confirm this interpretation, but the present results suggest that AFM spectroscopy might be not only sensitive to equilibrium density variations, but also to transient instabilities of water molecules between stable hydration layers. Stiff cantilevers are often preferred to match the conservative forces experienced by the tip and the MD-derived local density variations of the liquid [51,57,74,92]. Here, we used comparatively soft cantilevers, which have been proved effective to image weakly adsorbed ions [24,25,88] and may be sensitive to positional instabilities and potentially the mobility of the interfacial molecules found between the tip and the surface [67,100]. Previous work in a different system but with similar operating conditions [73] also reported discontinuities in both conservative and dissipative force components, with dissipative discontinuities interpreted as effective viscosity changes experienced by the tip as it expels solvation layers [73]. Although not directly comparable with the present work, those results also appear to support the idea that dissipative interactions can capture instabilities or transients associated with local variations in molecular dynamics at the interface. The interpretation of dissipative measurements may also be made more challenging by their non-equilibrium nature which makes them more sensitive to the precise experimental parameters and geometry at the point of

measurement compared to equilibrium AFM density measurements [51,57,74,92].

3.3. The impact of added salt

The presence of salt affects the hydration landscape of water-solid interfaces [28,88,101–103], modulating molecular processes including wetting [31,40,104], lubrication [28] and mineral growth [105]. Surprisingly, added ions do not appear to significantly affect the water densification as derived by the conservative component of AFM spectroscopic measurements [52,73,76,91,106]. Here, we probe the effect of Na^+ cations by conducting AFM imaging and spectroscopy on both facets of kaolinite in aqueous solutions containing 10 mM and 100 mM NaCl. The AFM measurements are complemented by MD simulations conducted for a system containing 1.2 M NaCl. The high concentration used in MD reflects the need to achieve meaningful statistics.

Taking as a reference the pure water-kaolinite interface, high resolution AM-AFM imaging shows that already at 10 mM, salt modifies the coordination of the water molecules at the surface interfering with their epitaxial organization (Fig. 4) (see also Supplementary Information Fig. S9 for more examples). The images appear noisier than in pure water over both facets with the appearance of local features and changes in contrast, albeit always in registry with the expected facet lattice. The spectroscopic curves are also more variable, as highlighted by the poorly defined molecular layers in the conservative datasets. The layering matches the density maxima as predicted by MD on both facets, but the statistical standard deviation over the curves indicates more variability. This larger variability can be due to variations in the interface sampled by the AFM probe due to the presence of ions. Additionally, a reduced cohesion of the water molecules [47] in the water hydrogen-bond network present on both surfaces is likely at play, an effect previously reported on similar mineral surfaces [25,28,88,107]. The hydration layers are still preserved both in the AFM conservative part of the spectroscopy curves and in the MD results, regardless of the added salt. The aluminol facet also retains its stronger and more cohesive first hydration layer. The clearest quantitative signature of the added ions is visible in the dissipative curves with a >30 % increase in dissipation across the interface compared to the pure water system, the absence of the maximum observed in pure water, and a progressively longer dissipation range towards the bulk liquid. This is consistent with ions affecting primarily the molecular dynamics of the interface while leaving the equilibrium water organisation largely unchanged [106]. Statistically, the fact that ions have little impact over the water density distribution should not come as a surprise; the number of water molecules exceeds that of ions by a ratio of 500–5000 to 1 in this study. It is notable that even these few ions can influence molecular motion between and along interfacial hydration layers.

Interestingly, increasing the ionic concentration to 100 mM NaCl partially stabilises the interface with images showing a better defined, more ordered contrast compared to 10 mM NaCl. A possible explanation comes from the fact that at larger salt concentration, the entropic effect of the ions in perturbing the ordered interfacial hydrogen bond network

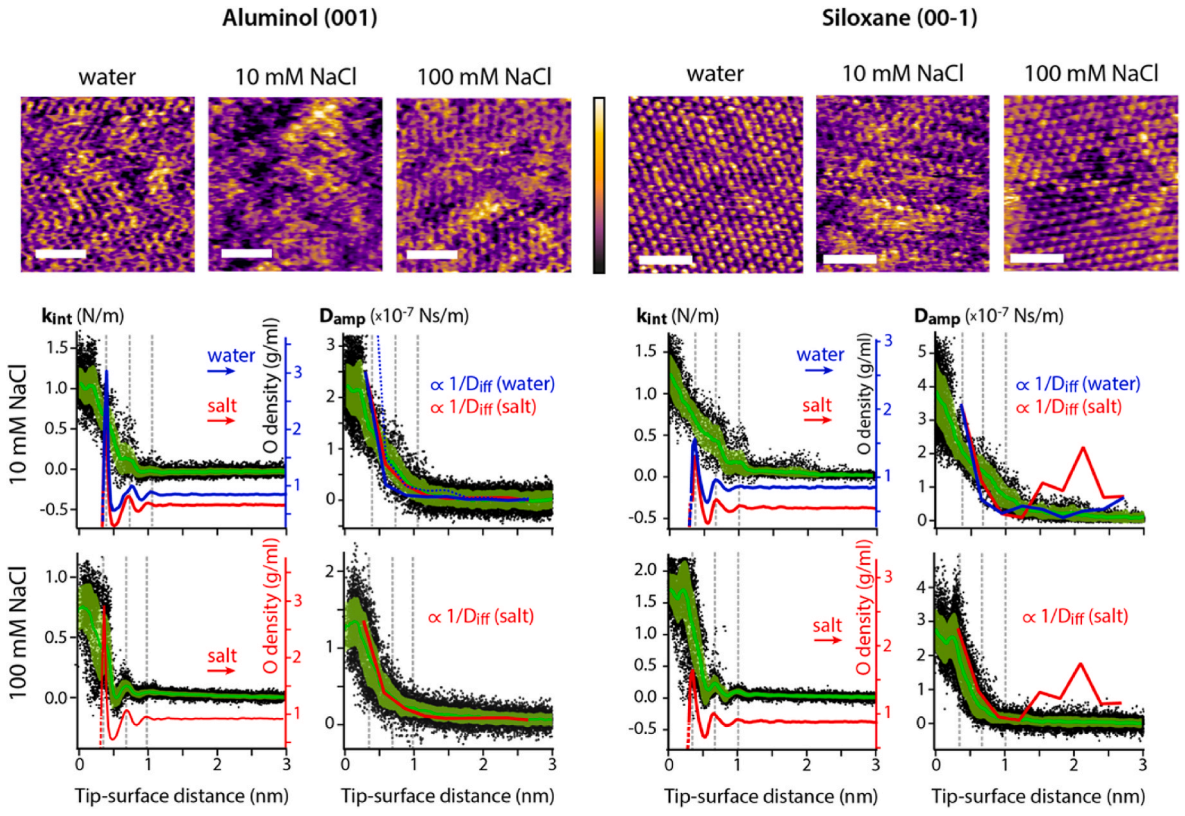

Fig. 4. Impact of salt on the hydration landscape of kaolinite. Experimental results at 10 and 100 mM NaCl are compared against simulations performed at 1.2 M NaCl. Comparative high-resolution AM-AFM images acquired in pure water, 10 mM and 100 mM NaCl over both facets (top). The imaging resolution is poorest at 10 mM, together with lower reproducibility in conservative curves and higher dissipation. Using the same scaling as in Fig. 3, the dissipative curves on aluminol suggest an intermediate simulated scenario between pure water scaled as in Fig. 3 (dashed blue), pure water scaled here for 10 mM (solid blue) and 1.2 M NaCl scaled for 10 mM (solid red). The effect is reversed when increasing the salt concentration to 100 mM NaCl presumably through the formation of ordered ionic domains (see Supplementary Fig. S9). Consistently, the conservative and dissipative components suggest a more stable interface with lower dissipation albeit on a longer range for aluminol. A hint of dissipation maximum is visible on the siloxane facet. The excellent agreement between AFM and MD also supports the idea of a more stable interface at 100 mM compared to 10 mM. The dotted grey lines represent the position of the water layers from the local maxima in simulated water oxygen density profiles. The scale bar represents 2.0 nm. The colour scale bar represents a height variation of ~0.6 nm. (For interpretation of the references to colour in this figure legend, the reader is referred to the Web version of this article.)

can be partially compensated by in-plane interactions between hydrated ions [108]. This greater stability favours the formation of ionic domains and a return to a more structured interface. Ordered ionic domains can occasionally be observed in both AFM and MD results (Supplementary Information, Fig. S9). Consistently, the conservative curves become more reproducible with smaller standard deviation compared to those obtained at low salt concentration and achieve an excellent agreement with MD results for both facets. The dissipation decreases again in magnitude after the associated curves reaching their highest values at 10 mM, with hints of an inter-layer maximum visible but only for the siloxane facet. In contrast, the spatial range of the dissipation increases mainly over the aluminol facet where MD diffusivity results predict a slower convergence to bulk value in the presence of salt (see also Fig. S8). The good agreement between the computational results with the experiments performed at 100 mM NaCl also suggests that higher salt concentrations have the effect of stabilising and ordering the hydrated interfacial structure.

Regardless of the molecular details of the interface, the fact that the steepest dissipative gradient is observed at 10 mM suggests a sharper but non-discrete transition from surface to bulk, supporting the experimental observations of small salt concentrations disfavouring an ordered solid-like layering of the fluid. This raises the possibility that the ionic effects well-known to affect interfacial processes on minerals [27,87,88] may also be driven by dissipative dynamical effects in the water. This would be consistent with the strong ionic sensitivity observed in shearing measurements [28] especially when the specific hydration landscape of a given surface precludes direct ionic adsorption [87]. Adding a small amount of salt (10 mM) would effectively results in a kind of 'slurry mixture' with lower densification and a concurrent increase in the number of dissipation channels experienced by the fluid molecules compared to a well-ordered interface. The effect is reduced in pure water and reversed when increasing the salt concentration high enough to allow the formation once again of well-stratified layers.

Finally, the fact that AFM images can capture dynamical interfacial effects at the interface even when no clear impact on the water equilibrium structure can be identified raises the question as to what high-resolution AFM images of immersed interface truly measure. The present results suggest a combination of equilibrium and non-equilibrium dynamical information.

4. Conclusions

In this study, we combine high-resolution AFM imaging and force spectroscopy with classical MD simulations to illustrate key differences in the hydration behaviour of the aluminol and siloxane facets of kaolinite particles immersed in water and NaCl solutions. The first hydration layer on the aluminol facet is denser and sits closer to the surface than over the siloxane facet. In contrast, the mobility of water molecules at the interface is reduced over a longer range at the aluminol facet, reaching bulk mobility over ~0.5 nm in pure water. Comparing AFM spectroscopic measurements with MD trajectories suggests that AFM can locally capture both the equilibrium molecular organisation of the interface as well as molecular dissipative instabilities between stable locations. Adding salt disrupts the interfacial hydrogen bond network of water molecules with the most dramatic effect visible in increased AFM dissipation at 10 mM. At higher salt concentration, the ions appear to form stable mesoscale domains, allowing more ordered and stable interfaces. A similar phenomenon is likely to occur between kaolinite platelets in salt-saturated environments. The present results have been obtained using naturally occurring kaolinite powder rather than synthetic particles. The higher frequency of defects and topographical singularities in natural kaolinite may be relevant to geochemical phenomena and technology often based on the natural mineral. The differences in the hydration structure and its dynamics on the two kaolinite facets could be exploited to further support advanced technological devices. For example, the diverse water affinity and structural organisation on the two facets may be selectively used as a natural adsorbent to remove specific pollutants of different hydrophilicity from wastewater [109]. Further studies are needed to investigate the effect of different cations and extend the current findings to other ionic species, including for potential applications in the fields of energy and the design of the 'ultimate green' wastewater and nuclear waste treatment.

CRediT authorship contribution statement

Clodomiro Cafolla: Writing – review & editing, Writing – original draft, Methodology, Investigation, Formal analysis, Conceptualization. **Tai Bui:** Software, Methodology, Investigation, Formal analysis. **Tran Thi Bao Le:** Software, Investigation. **Andrea Zen:** Software, Methodology. **Weparn J. Tay:** Supervision, Conceptualization. **Alberto Striolo:** Writing – review & editing, Validation, Supervision, Conceptualization. **Angelos Michaelides:** Writing – review & editing, Validation, Supervision, Methodology, Conceptualization. **Hugh Christopher Greenwell:** Writing – review & editing, Validation, Supervision, Methodology, Funding acquisition, Conceptualization. **Kislon Voïtchovsky:** Writing – review & editing, Writing – original draft, Visualization, Validation, Supervision, Methodology, Funding acquisition, Formal analysis, Conceptualization.

Declaration of competing interest

The authors declare the following financial interests/personal relationships which may be considered as potential competing interests: All authors reports financial support was provided by BP. Kislon Voitchovsky reports financial support was provided by Engineering and Physical Sciences Research Council. If there are other authors, they declare that they have no known competing financial interests or personal relationships that could have appeared to influence the work reported in this paper.

Data availability

Data will be made available on request.

Acknowledgements

C. C. is grateful to the Physics Dept Durham University (Developing Talent Scheme) and to the Durham University Institute of Advanced Studies for the financial support. K.V. gratefully acknowledges support from the Engineering and Physical Sciences Research Council (Fellowship EP/S028234/1).

Appendix A. Supplementary data

Supplementary data to this article can be found online at https://doi.org/10.1016/j.mtphys.2024.101504.

References

[1] W. Hao, K. Mänd, Y. Li, D.S. Alessi, P. Somelar, M. Moussavou, A.E. Romashkin, A. Lepland, K. Kirsimäe, N.J. Planavsky, K.O. Konhauser, The kaolinite shuttle links the great oxidation and Lomagundi events, Nat. Commun. 12 (2021) 2944.
[2] M.E. Awad, A. López-Galindo, M. Setti, M.M. El-Rahmany, C.V. Iborra, Kaolinite in pharmaceutics and biomedicine, Int. J. Pharm. 533 (2017) 34–48.
[3] F. González Sánchez, F. Jurányi, T. Gimmi, L. Van Loon, T. Unruh, L.W. Diamond, Translational diffusion of water and its dependence on temperature in charged and uncharged clays: a neutron scattering study, J. Chem. Phys. 129 (2008): 174706.
[4] D. Trabattoni, P. Gatto, A.L. Bartorelli, A new kaolin-based hemostatic bandage use after coronary diagnostic and interventional procedures, Int. J. Cardiol. 156 (2012) 53–54.
[5] S. Zhu, S.L. Diamond, Contact activation of blood coagulation on a defined kaolin/collagen surface in a microfluidic assay, Thromb. Res. 134 (2014) 1335–1343.

[6] N. Santha, P. Cubillas, A. Saw, H. Brooksbank, C.H. Greenwell, Chemical force microscopy study on the interactions of COOH functional groups with kaolinite surfaces: implications for enhanced oil recovery, Minerals 7 (2017) 250.

[7] T. Puntervold, A. Mamonov, Z. Aghaeifar, G.O. Frafjord, G.M. Moldestad, S. Strand, T. Austad, Role of kaolinite clay minerals in enhanced oil recovery by low salinity water injection, Energy Fuels 32 (2018) 7374–7382.

[8] S.A. Sleptsova, S. Laukkanen, N.P. Gladkina, V.I. Fedoseeva, A.A. Okhlopkova, L. A. Grigoryeva, Effect of kaolinite on the properties and structure of PTFE, AIP Conf. Proc. 2053 (2018): 040092.

[9] C.F. Revelo, H.A. Colorado, 3D printing of kaolinite clay ceramics using the Direct Ink Writing (DIW) technique, Ceram. Int. 44 (2018) 5673–5682.

[10] A. Aras, The change of phase composition in kaolinite- and illite-rich clay-based ceramic bodies, Appl. Clay Sci. 24 (2004) 257–269.

[11] S. Sivachidambaram, S.M. Rao, Iodide retention by modified kaolinite in the context of safe disposal of high level nuclear waste, J. Hazardous, Toxic, Radioact. Waste 16 (2012) 192–200.

[12] I.M. El-Naggar, S.A. Ahmed, N. Shehata, E.S. Sheneshen, M. Fathy, A. Shehata, A novel approach for the removal of lead (II) ion from wastewater using kaolinite/smectite natural composite adsorbent, Appl. Water Sci. 9 (2019) 7.

[13] C. Detellier, Functional kaolinite, Chem. Rec. 18 (2018) 868–877.

[14] N. Molaei, O. Bashir Wani, E.R. Bobicki, A comparative study of biopolymer adsorption on model anisotropic clay surfaces using quartz crystal microbalance with dissipation (QCM-D), J. Colloid Interface Sci. 615 (2022) 543–553.

[15] X.L. Hu, A. Michaelides, The kaolinite (0 0 1) polar basal plane, Surf. Sci. 604 (2010) 111–117.

[16] T.T.B. Le, A.R. Finney, A. Zen, T. Bui, W.J. Tay, K. Chellappah, A. Michaelidis, M. Salvalaglio, A. Striolo, Mesoscale simulations reveal how salt influences clay particles agglomeration in aqueous Ddispersions, J. Chem. Theor. Comput. 20 (2024) 1612–1624.

[17] S. Raynaud, G. Vasseur, B. Célérier, D. Loggia, M. Ghoreychi, M.H. Mathon, F. Mazerolle, Experimental study of the relation between the permeability of kaolinite and its deformation at micro and macro scale, Int. J. Rock Mech. Min. Sci. 47 (2010) 559–567.

[18] J. Ikhsan, B.B. Johnson, J.D.A. Wells, Comparative study of the adsorption of transition metals on kaolinite, J. Colloid Interface Sci. 217 (1999) 403–410.

[19] J. Rosenqvist, P. Persson, S. Sjöberg, Protonation and charging of nanosized gibbsite (α-Al(OH)3) particles in aqueous suspension, Langmuir 18 (2002) 4598–4604.

[20] R. Weerasooriya, B. Dharmasena, D. Aluthpatabendi, Copper–gibbsite interactions: an application of 1-pK surface complexation model, Colloids Surf. A Physicochem. Eng. Asp. 170 (2000) 65–77.

[21] M. Alkan, O. Demirbaş, M. Doğan, Electrokinetic properties of kaolinite in mono- and multivalent electrolyte solutions, Microporous Mesoporous Mater. 83 (2005) 51–59.

[22] Y. Yukselen, A. Kaya, Zeta Potential of kaolinite in the presence of alkali, alkaline earth and hydrolyzable metal ions, Water, Air, Soil Pollut. 145 (2003) 155–168.

[23] J. Lützenkirchen, A. Abdelmonem, R. Weerasooriya, F. Heberling, V. Metz, R. Marsac, Adsorption of dissolved aluminum on sapphire-c and kaolinite: implications for points of zero charge of clay minerals, Geochem. Trans. 15 (2014) 1–14.

[24] C. Cafolla, W. Foster, K. Voïtchovsky, Lubricated friction around nanodefects, Sci. Adv. 6 (2020): eaaz3673.

[25] C. Cafolla, K. Voïtchovsky, Real-time tracking of ionic nano-domains under shear flow, Sci. Rep. 11 (2021): 19540.

[26] D. Bastos-González, L. Pérez-Fuentes, C. Drummond, J. Faraudo, Ions at interfaces: the central role of hydration and hydrophobicity, Curr. Opin. Colloid Interface Sci. 23 (2016) 19–28.

[27] M. Ricci, W. Trewby, C. Cafolla, K. Voïtchovsky, Direct observation of the dynamics of single metal ions at the interface with solids in aqueous solutions, Sci. Rep. 7 (2017): 43234.

[28] C. Cafolla, K. Voïtchovsky, Lubricating properties of single metal ions at interfaces, Nanoscale 10 (2018) 11831–11840.

[29] C. Cafolla, K. Voïtchovsky, Impact of water on the lubricating properties of hexadecane at the nanoscale, Nanoscale 12 (2020) 14504–14513.

[30] J. Krim, Friction and energy dissipation mechanisms in adsorbed molecules and molecularly thin films, Adv. Phys. 61 (2012) 155–323.

[31] F. Mugele, B. Bera, A. Cavalli, I. Siretanu, A. Maestro, M. Duits, M. Cohen-Stuart, D. van den Ende, I. Stocker, I. Collins, Ion adsorption-induced wetting transition in oil-water-mineral systems, Sci. Rep. 5 (2015): 10519.

[32] S.R. Van Lin, K.K. Grotz, I. Siretanu, N. Schwierz, F. Mugele, Ion-specific and pH-dependent hydration of mica-electrolyte interfaces, Langmuir 35 (2019) 5737–5745.

[33] A. Klaassen, F. Liu, S. de Beer, D. van den Ende, and F. Mugele. Atomic force microscopy of confined liquids using the thermal bending fluctuations of the cantilever. Phys. Rev. E 87, 62406.

[34] N. Kumar, C. Zhao, A. Klaassen, D. van den Ende, F. Mugele, I. Siretanu, Characterization of the surface charge distribution on kaolinite particles using high resolution atomic force microscopy, Geochem. Cosmochim. Acta 175 (2016) 100–112.

[35] B.A. Sakharov, V.A. Drits, D.K. McCarty, G.M. Walker, Modeling powder x-ray diffraction patterns of the clay minerals society kaolinite standards: KGA-1, KGA-1b, and KGa-2, Clay Clay Miner. 64 (2016) 314–333.

[36] S. Komarneni, C.A. Fyfe, G.J. Kennedy, Order-disorder in 1:1 type clay minerals by solid-state 27Al and 29Si magic-angle-spinning NMR spectroscopy, Clay Miner. 20 (1985) 327–334.

[37] N. Sahai, S.A. Carroll, S. Roberts, P.A. O'Day, X-Ray absorption spectroscopy of strontium(II) coordination: II. Sorption and precipitation at kaolinite, amorphous silica, and goethite surfaces, J. Colloid Interface Sci. 222 (2000) 198–212.

[38] M. Raupach, P.F. Barron, J.G. Thompson, Nuclear magnetic resonance, infrared, and X-ray powder diffraction study of dimethylsulfoxide and dimethylselenoxide intercalates with kaolinite, Clay Clay Miner. 35 (1987) 208–219.

[39] A. Doi, M. Khosravi, M. Ejtemaei, T.A.H. Nguyen, A.V. Nguyen, Specificity and affinity of multivalent ions adsorption to kaolinite surface, Appl. Clay Sci. 190 (2020): 105557.

[40] A. Doi, M. Ejtemaei, A.V. Nguyen, Effects of ion specificity on the surface electrical properties of kaolinite and montmorillonite, Miner. Eng. 143 (2019): 105929.

[41] B. Jagoda-Cwiklik, B. Rotenberg, P. Turq, Structure and dynamics of water at a clay surface from molecular dynamics simulation, Phys. Chem. Chem. Phys. 10 (2008) 4802–4813.

[42] D. Tunega, M.H. Gerzabek, H. Lischka, Ab initio molecular dynamics study of a monomolecular water layer on octahedral and tetrahedral kaolinite surfaces, J. Phys. Chem. B 108 (2004) 5930–5936.

[43] M.R. Warne, N.L. Allan, T. Cosgrove, Computer simulation of water molecules at kaolinite and silica surfaces, Phys. Chem. Chem. Phys. 2 (2000) 3663–3668.

[44] B. Liu, M. Dai, I. Ali, S. Li, L. Sun, C. Peng, I. Naz, Molecular insights on the influence of temperature and metal ions on the hydration of kaolinite (001) surface, Mol. Simulat. 47 (2021) 1029–1036.

[45] T. Underwood, V. Erastova, H.C. Greenwell, Wetting effects and molecular adsorption at hydrated kaolinite clay mineral surfaces, J. Phys. Chem. C 120 (2016) 11433–11449.

[46] C. Cafolla, Lubricated Friction at the Nano and Mesoscale, University of Durham, 2020.

[47] G.R. Quezada, R.E. Rozas, P.G. Toledo, *Ab-initio* calculations of partial charges at kaolinite edge sites and molecular dynamics simulations of cation adsorption in saline solutions at and above the pH of zero charge, J. Phys. Chem. C 123 (2019) 22971–22980.

[48] D. Argyris, P.D. Ashby, A. Striolo, Structure and orientation of interfacial water determine atomic force microscopy results: insights from molecular dynamics simulations, ACS Nano 5 (2011) 2215–2223.

[49] D. Argyris, A. Phan, A. Striolo, P.D. Ashby, Hydration structure at the α-Al_2O_3 (0001) surface: insights from experimental atomic force spectroscopic data and atomistic molecular dynamics simulations, J. Phys. Chem. C 117 (2013) 10433–10444.

[50] K. Umeda, K. Kobayashi, T. Minato, H. Yamada, Atomic-level viscosity distribution in the hydration layer, Phys. Rev. Lett. 122 (2019) 116001.

[51] A. Klaassen, F. Liu, F. Mugele, I. Siretanu, Correlation between electrostatic and hydration forces on silica and gibbsite surfaces: an atomic force microscopy study, Langmuir 38 (2022) 914–926.

[52] I. Siretanu, D. Van Den Ende, F. Mugele, Atomic structure and surface defects at mineral-water interfaces probed by: in situ atomic force microscopy, Nanoscale 8 (2016) 8220–8227.

[53] Y. Guo, X. Yu, Characterizing the surface charge of clay minerals with atomic force microscope (AFM), AIMS Mater. Sci. 4 (2017) 582–593.

[54] N. Kumar, M.P. Andersson, D. Van Den Ende, F. Mugele, I. Siretanu, Probing the surface charge on the basal planes of kaolinite particles with high-resolution atomic force microscopy, Langmuir 33 (2017) 14226–14237.

[55] J. Chang, B. Liu, J.S. Grundy, H. Shao, R.M. Zhen Li, Q. Liu, Z. Xu, Probing specific adsorption of electrolytes at kaolinite-aqueous interfaces by atomic force microscopy, J. Phys. Chem. Lett. 12 (2021) 2406–2412.

[56] V. Gupta, J.D. Miller, Surface force measurements at the basal planes of ordered kaolinite particles, J. Colloid Interface Sci. 344 (2010) 362–371.

[57] H. Söngen, B. Reischl, K. Miyata, R. Bechstein, P. Raiteri, A.L. Rohl, J.D. Gale, T. Fukuma, A. Kühnle, Resolving point defects in the hydration structure of calcite (10.4) with three-dimensional atomic force microscopy, Phys. Rev. Lett. 120 (2010): 16101.

[58] E.J. Miller, W. Trewby, A.F. Payam, L. Piantanida, C. Cafolla, K. Voïtchovsky, Sub-nanometer resolution imaging with amplitude-modulation tomic force microscopy in liquid, J. Vis. Exp. 118 (2016): e54924.

[59] E.J. Miller, K. Voïtchovsky, M. Staykova, Substrate-led cholesterol extraction from supported lipid membranes, Nanoscale 10 (2018) 16332–16342.

[60] M. Burkhardt, A. Jedaa, M. Novak, A. Ebel, K. Voïtchovsky, F. Stellacci, A. Hirsch, M. Hali, Concept of a molecular charge storage dielectric layer for Organic thin-film memory transistors, Adv. Mater. 22 (2010) 2525–2528.

[61] M. Iwasaki, Y. Matsudaira, K. Takeda, M. Ito, E. Miyamoto, T. Yara, T. Uehara, M. Hori, Roles of oxidizing species in a nonequilibrium atmospheric-pressure pulsed remote O2/N2 plasma glass cleaning process, J. Appl. Phys. 103 (2008): 023303.

[62] H.J. Butt, M. Jaschke, Calculation of thermal noise in atomic force microscopy, Nanotechnology 6 (1995) 1.

[63] C. Cafolla, A.F. Payam, K. Voïtchovsky, A non-destructive method to calibrate the torsional spring constant of atomic force microscope cantilevers in viscous environments, J. Appl. Phys. 124 (2018): 154502.

[64] C. Cafolla, K. Voïtchovsky, A. Farokh Payam, Simultaneous quantification of Young's modulus and dispersion forces with nanoscale spatial resolution, Nanotechnology 34 (2023): 505714.

[65] V. Pini, B. Tiribilli, C. Maria, C. Gambi C, M. Vassalli, Dynamical characterization of vibrating AFM cantilevers forced by photothermal excitation, Phys. Rev. B 81 (2010): 054302.

[66] F. Lavini, F. Cellini, M. Rejhon, J. Kunc, C. Berger, W. de Heer, E. Riedo, Atomic force microscopy phase imaging of epitaxial graphene films, J. Phys. Materials 3 (2020): 024005.
[67] K. Voïtchovsky, J.J. Kuna, S. Antoranz Contera, E. Tosatti, F. Stellacci, Direct mapping of the solid–liquid adhesion energy with subnanometre resolution, Nat. Nanotechnol. 5 (2010) 401–405.
[68] C. Dohno, S. Makishi, K. Nakatani, S. Contera, Amphiphilic DNA tiles for controlled insertion and 2D assembly on fluid lipid membranes: the effect on mechanical properties, Nanoscale 9 (2017) 3051–3058.
[69] J.B. McClimon, A.C. Lang, Z. Milne, N. Garabedian, A.C. Moore, J. Hilbert, F. Mangolini, J.R. Lukes, D.L. Burris, M.L. Taheri, J. Fontaine, R.W. Carpick, Investigation of the mechanics, composition, and functional behavior of thick tribofilms formed from silicon- and oxygen-containing hydrogenated amorphous carbon, Tribol. Lett. 67 (2019) 48.
[70] S. Hofmann, K. Voïtchovsky, P. Spijker, M. Schmidt, T. Stumpf, Visualising the molecular alteration of the calcite (104) – water interface by sodium nitrate, Sci. Rep. 6 (2016): 21576.
[71] O. Teschke, E.F. Souza, E.F. Atomic, Force microscopy improved resolution employing large scanning speeds: effects of the double relaxation time, Rev. Sci. Instrum. 69 (1998) 3588–3592.
[72] O. Teschke, E.F. De Souza, G. Ceotto, G. Double layer relaxation measurements using atomic force microscopy, Langmuir 15 (1999) 4935–4939.
[73] S. De Beer, D. Van den Ende, F. Mugele, Dissipation and oscillatory solvation forces in confined liquids studied by small-amplitude atomic force spectroscopy, Nanotechnology 21 (2010): 325703.
[74] T. Fukuma, R. Garcia, Atomic- and molecular-resolution mapping of solid-liquid interfaces by 3D atomic force microscopy, ACS Nano 12 (2018) 11785–11797.
[75] T. Fukuma, Y. Ueda, S. Yoshioka, H. Asakawa, Atomic-scale distribution of water molecules at the mica-water interface visualized by three-dimensional scanning Force microscopy, Phys. Rew. Lett. 104 (2010): 016101.
[76] F. Liu, A. Klaassen, C. Zhao, F. Mugele, D. Van Den Ende, Electroviscous dissipation in aqueous electrolyte films with overlapping electric double layers, J. Phys. Chem. B 122 (2018) 933–946.
[77] S. Plimpton, Fast parallel algorithms for short-range molecular dynamics, J. Comput. Phys. 117 (1995) 1–19.
[78] D.L. Bish, Rietveld refinement of the kaolinite structure at 1.5 K, Clay Clay Miner. 41 (1993) 738–744.
[79] R.T. Cygan, J.J. Liang, A.G. Kalinichev, Molecular models of hydroxide, oxyhydroxide, and clay phases and the development of a general force field, J. Phys. Chem. B 108 (2004) 1255–1266.
[80] M. Pouvreau, J.A. Greathouse, R.T. Cygan, A.G. Kalinichev, Structure of hydrated kaolinite edge surfaces: DFT results and further development of the ClayFF classical force field with metal-O-H angle bending terms, J. Phys. Chem. C 123 (2019) 11628–11638.
[81] M. Pouvreau, J.A. Greathouse, R.T. Cygan, A.G. Kalinichev, Structure of hydrated gibbsite and brucite edge surfaces: DFT results and further development of the ClayFF classical force field with metal-O-H angle bending terms, J. Phys. Chem. C 121 (2017) 14757–14771.
[82] H.J.C. Berendsen, J.R. Grigera, T.P. Straatsma, The missing term in effective pair potentials1, J. Phys. Chem. 91 (1987) 6269–6271.
[83] A. Zen, T. Bui, T.T. Bao Le, W.J. Tay, K. Chellappah, I.R. Collins, R.D. Rickman, A. Striolo, Angelos Michaelides, Long-range ionic and short-range hydration effects govern strongly anisotropic clay nanoparticle interactions, J. Phys. Chem. C 126 (2022) 8143–8151.
[84] D.E. Smith, L.X. Dang, Computer simulations of NaCl association in polarizable water, J. Chem. Phys. 100 (1998) 3757.
[85] R. Hockney, J. Eastwood, Computer Simulation Using Particles, CRC Press, Boca Raton, 2021.
[86] S. Nosé, M.L. Klein, Constant pressure molecular dynamics for molecular systems, Mol. Phys. 50 (1983) 1055–1076.
[87] M. Ricci, P. Spijker, F. Stellacci, J.F. Molinari, K. Voïtchovsky, Direct visualization of single ions in the stern layer of calcite, Langmuir 29 (2013) 2207–2216.
[88] M. Ricci, P. Spijker, K. Voïtchovsky, Water-induced correlation between single ions imaged at the solid-liquid interface, Nat. Commun. 5 (2014) 4400.
[89] G. Varga, The structure of kaolinite and metakaolinite, JSBCM 59 (2007) 1. http://en.epitoanyag.org.hu/static/upload/10.14382epitoanyag-jsbcm.2007.2.pdf. July 2022.
[90] R.A. Young, A.W. Hewat, Verification of the triclinic crystal structure of kaolinite, Clay Clay Miner. 36 (1988) 225–232.
[91] F. Liu, S. de Beer, D. van den Ende, F. Mugele, Atomic force microscopy of confined liquids using the thermal bending fluctuations of the cantilever, Phys. Rev. E 87 (2013): 62406.
[92] C. Marutschke, D. Walters, J. Cleveland, I. Hermes, R. Bechstein, A. Kühnle, Three-dimensional hydration layer mapping on the (10.4) surface of calcite using amplitude modulation atomic force microscopy, Nanotechnology 25 (2014): 335703.
[93] V. Marry, B. Rotenberg, P. Turq, Structure and dynamics of water at a clay surface from molecular dynamics simulation, Phys. Chem. Chem. Phys. 10 (2008) 4802–4813.
[94] F. Liu, C. Zhao, F. Mugele, D. van den Ende, Amplitude modulation atomic force microscopy, is acoustic driving in liquid quantitatively reliable? Nanotechnology 26 (2015): 385703.
[95] R.A.L. Jones, Soft Condensed Matter, Oxford University Press, 2002.
[96] G.B. Kaggwa, P.C. Nalam, J.I. Kilpatrick, N.D. Spencer, S.P. Jarvis, Impact of hydrophilic/hydrophobic surface chemistry on hydration forces in the absence of confinement, Langmuir 28 (2012) 6589–6594.
[97] K. Voïtchovsky, High-resolution AFM in liquid: what about the tip? Nanotechnology 26 (2015): 100501.
[98] S.M.R. Akrami, H. Nakayachi, T. Watanabe-Nakayama, H. Asakawa, T. Fukuma, Significant improvements in stability and reproducibility of atomic-scale atomic force microscopy in liquid, Nanotechnology 25 (2014): 455701.
[99] A.N. Pisarchik, U. Feudel, D.K. Campbell, Control of multistability, Phys. Rep. 540 (2014) 167–218.
[100] D. Ortiz-Young, H.C. Chiu, S. Kim, K. Voïtchovsky, E. Riedo, The interplay between apparent viscosity and wettability in nanoconfined water, Nat. Commun. 4 (2013) 2482.
[101] I. Waluyo, C. Huang, D. Nordlund, U. Bergmann, T.M. Weiss, L.G.M. Pettersson, A. Nilsson, The structure of water in the hydration shell of cations from x-ray Raman and small angle x-ray scattering measurements, J. Chem. Phys. 134 (2011): 064513.
[102] C. Park, P.A. Fenter, K.L. Nagy, N.C. Sturchio, Hydration and distribution of ions at the mica-water interface, Phys. Rev. Lett. 97 (2006): 016101.
[103] T. Sayer, S.J. Cox, Macroscopic surface charges from microscopic simulations, J. Chem. Phys. 153 (2020): 164709.
[104] K.C. Jena, D.K. Hore, Variation of ionic strength reveals the interfacial water structure at a charged mineral surface, J. Phys. Chem. C 113 (2009) 15364–15372.
[105] R. Milke, R. Dohmen, H.W. Becker, R. Wirth, Growth kinetics of enstatite reaction rims studied on nano-scale, Part I: Methodology, microscopic observations and the role of water, Contrib. Mineral. Petrol. 154 (2007) 519–533.
[106] I. Siretanu, S.R. Van Lin, F. Mugele, Ion adsorption and hydration forces: a comparison of crystalline mica vs. amorphous silica surfaces, Faraday Discuss 246 (2023) 274–295.
[107] M.L. Schlegel, K.L. Nagy, P. Fenter, L. Cheng, N.C. Sturchio, S.D. Jacobsen, Cation sorption on the muscovite (0 0 1) surface in chloride solutions using high-resolution X-ray reflectivity, Geochem. Cosmochim. Acta 70 (2006) 3549–3565.
[108] J. Wang, H. Li, M. Tavakol, A. Serva, B. Nener, G. Parish, M. Salanne, G.G. Warr, K. Voïtchovsky, R. Atkin, Ions adsorbed at amorphous solid/solution interfaces form wigner crystal-like structures, ACS Nano 18 (2023) 1181–1194.
[109] S. Mustapha, M.M. Ndamitso, A.S. Abdulkareem, J.O. Tijani, A.K. Mohammed, D. T. Shuai, Potential of using kaolin as a natural adsorbent for the removal of pollutants from tannery wastewater, Heliyon 5 (2019): e02923.